Analytical and Bioanalytical Chemistry (2023) 415:703–713
https://doi.org/10.1007/s00216-022-04461-1

RESEARCH PAPER

Label-free ultra-sensitive colorimetric detection of hepatitis E virus based on oxidase-like activity of MnO_2 nanosheets

Naveed Alam[1] · Chandan Hunsur Ravikumar[2] · Muralikrishna Sreeramareddygari[3] · Mithran Somasundrum[4] · Werasak Surareungchai[1,5,6]

Received: 3 September 2022 / Revised: 18 November 2022 / Accepted: 22 November 2022 / Published online: 5 December 2022

Abstract

Hepatitis E virus (HEV) is an evolving infectious entity that causes viral hepatitis infections worldwide. Current routine methods of identifying and diagnosing HEV are someway laborious and costly. Based on the biomimicking oxidase-like activity of MnO_2 nanosheets, we designed a label-free, highly sensitive colorimetric sensing technique for HEV detection. The prepared MnO_2 catalyst displays intrinsic biomimicking oxidase-like catalytic activity and efficiently oxidizes the 3,3′,5,5′-tetramethylbenzidine (TMB) substrate from colorless to blue colored oxidized TMB (oxTMB) product which can be measured at 652 nm by UV–visible spectrum. When the HEV-DNA was added, DNA adsorbed easily on MnO_2 surface through physical adsorption and electrostatic interaction which hinders the oxidase-like catalytic activity of MnO_2. Upon the introduction of target, the HEV target DNA binds with its complementary ssDNA on the surface of MnO_2, the hybridized DNA releases from the surface of MnO_2, which leads to recovery of oxidase-like catalytic activity of MnO_2. This strategy was applied to construct a colorimetric technique for HEV detection. The approach works in the linear range of 1 fM–100 nM DNA concentration with the limit of detection (LOD) of 3.26 fM (S/N = 3) and quantitative limit (LOQ) of 36.08 fM. The TMB-MnO_2 platform was highly selective for HEV target DNA detection when compared with potential interferences. Result of serum sample analysis demonstrates that this sensing system can be used for clinical diagnostic applications.

Keywords Hepatitis E virus · MnO_2 · Nanozymes · DNA · Oxidase-mimicking · Biosensors

✉ Werasak Surareungchai
werasak.sur@kmutt.ac.th

1 School of Bioresources and Technology, King Mongkut's University of Technology Thonburi, Bangkok 10150, Thailand

2 Centre for Nano and Material Sciences, Jain University, Jain Global Campus, Jakkasandra Post, Ramangaram Dist, Karnataka 562112, India

3 Pilot Plant Development and Training Institute, King Mongkut's University of Technology Thonburi, Bangkok10150, Thailand

4 Biosciences and System Biology Team, Biochemical Engineering and System Biology Research Group, National Center for Genetic Engineering and Biotechnology, National Science and Technology Development Agency at KMUTT (Bangkhuntien Campus), Bangkok 10150, Thailand

5 Nanoscience & Nanotechnology Graduate Programme, Faculty of Science, King Mongkut's University of Technology Thonburi, Bangkok 10140, Thailand

6 Analytical Sciences and National Doping Test Institute, Mahidol University, Bangkok 10400, Thailand

Introduction

Hepatitis E virus (HEV) is an empirically transmitted RNA virus that causes outbreaks or various sporadic diseases [1]. The HEV major genotypes (G1 to G4) are well-recognized for infection around the world. However, the zoonotic nature of G3 and G4 genotypes can infect animals. HEV was first reported in Asia and Africa for causing acute hepatitis by fecal–oral transmission, while later on it has been found endemic in Japan and Europe [2]. HEV infects annually more than 20 million people worldwide, and for more than 3 million people it leads to hepatitis E [3]. According to WHO, about 44,000 people died from HEV infection in 2015 [4]. Several clinical diagnoses of HEV disease rely on antibody-based detection procedures and techniques involving RNAs such as reverse transcription-polymerase chain reaction (RT-PCR) and enzyme immunoassay, respectively [5]. Despite the sensitivity and specificity of RT-PCR techniques, there are still limitations due to their high cost and rate of false-positive

detection. A fast and early detection is required to prevent and monitor the outbreak. This demands to develop a biosensor that could ideally quantify an individual viral particle [6]. Therefore, in order to ensure public health safety, it is vital to develop sensitive and reliable techniques for HEV detection. In the pandemic era, there is a great need for high-accuracy biosensors, which depends on the design of promising biosensing materials using composite sensing techniques.

Recently, the use of nanomaterials (NPs) as nanoenzymes that can mimic the intrinsic catalytic functional property similar to natural enzyme gains a widespread attention. Due to their unique structures, high stabilities and simple facile synthesis, as well as remarkable catalytic activities of NPs, gained more interest [7]. A high efficiency for the adsorption of numerous small molecules and biomolecules, such as amino acids, proteins, DNA, and ions present in biological media, can be attained by NPs with high specific surface area [8]. Additionally, nanozymes have been combined with biomolecules and biopolymers for a variety of clinical and sensing applications [9]. These widespread features make the nanozymes as the physicochemical entity alternative to some of natural enzyme with more or else similar properties [10, 11].

In addition, notably, some two-dimensional (2D) materials/nanosheets, such as graphene oxides [12], metal disulfides [13], metal oxides [14, 15], and carbon nitride [16], mimic the action of natural enzymes in widespread applications for biosensing [17, 18] and chemosensing [19, 20]. Furthermore, 2D nanosheets can create layered nanostructures that are more chemically and thermally stable than natural enzymes, which may open up new opportunities for new industrial and clinical applications [21]. As a result, 2D nanomaterials can be used to create artificial enzymes with target analyte selectivity and many catalytic active sites, which will boost the catalytic activity. This is made possible by the unique properties of having an ultra-large surface area and flexibility. MnO_2 nanosheet (NS), is widely reported as a novel two-dimensional (2D) single-layer inorganic nanomaterial. With the precise material tailoring, an enzyme mimic can be produced that has great oxidase-like properties, low toxicity, high stability, and good water dispersion [22, 23]. MnO_2 nanoparticles have been widely used in biosensing, bioimaging, delivery of single stranded DNA (ssDNA), and drugs [7, 24]. MnO_2 nanosheets, in contrast to other biomimetic oxidases, have a unique capacity for decomposition, providing a substitute for the detection of glutathione [25], oxalate, DNA [26], ascorbic acid, and alkaline phosphatase [27]. In this case, the catalytic substrates 2,2′-azino-bis (3-ethylbenzthiazoline-6-sulfonate) diammonium salt (ABTS), 3,3′,5,5′-tetramethylbenzidine (TMB), and o-toluidine (OT) are oxidized to produce distinctive color change during reaction with MnO_2 nanosheets [28]. MnO_2 nanosheets could therefore be employed for colorimetric sensing and have higher compatibility with a number of biosensing pathways.

Here, based on the oxidase-like activity of MnO_2 nanosheets, we designed for the first time a simple, label-free, cost-effective, and rapid colorimetric technique for the extremely sensitive detection of HEV. To achieve a more rapid and facile sensing platform, the DNA oligonucleotides were directly adsorbed on the surface of MnO_2 to simplify our assay design. The multi-step sensor fabrication processes avoided that are usually associated with DNA hybridization-based assays. With a characteristic absorption peak at 652 nm, the MnO_2 nanosheets in this sensing platform may directly catalyze the oxidation of TMB, turning it from colorless to blue oxTMB and exhibiting excellent biomimetic oxidase-like activity. The facile synthesized MnO_2 nanosheet was characterized using structural and crystalline details to confirm the formation of sheet like structure using X-ray diffraction (XRD) and transmission electron microscopy (TEM). Further, the atomic force microscopy was carried out to confirm the adsorption of ssDNA on to the MnO_2 sheets. This colorimetric approach has great sensing performance with lower limit of detection and high sensitivity and selectivity. Low-toxic, well-biocompatible, and readily synthesized biosensors are very promising for using in clinical samples to diagnose diseases.

Materials and methods

Materials

The chemicals used in this investigation were of the analytical grade and were utilized directly without any further purification. Potassium permanganate was acquired from Sinopharm Chemical Reagent Co., Ltd, China. Potassium dihydrogen phosphate (≥ 98%), di-potassium hydrogen phosphate anhydrous (≥ 98%), acetic acid (99.8%), and ethanol (99.9%) were obtained from Merck, USA. Sodium acetate (99–101%) was purchased from Ajax Fine Chem. 3,3′,5,5′-tetramethylbenzidine (> 98%) was procured from Tokyo Chemical Industry, Japan, and human serum from Sigma-Aldrich, USA. All the oligonucleotides were acquired from Integrated DNA Technologies Ltd., Singapore, and were used without additional purification. For all the experiments, Milli-Q water was used. The sequences of oligonucleotide [29] used in this study are as follows:

o HEV capture probe sequences (18 bases)
p 5′-GGTGGTTTCTGGGGTGAC-3′
q HEV target probe sequences (51 bases)
r 5′-GGATTGCGAAGGGCTGAGAATCAACCCGGT CACCCCAGAAACCA CCGCCGG-3′

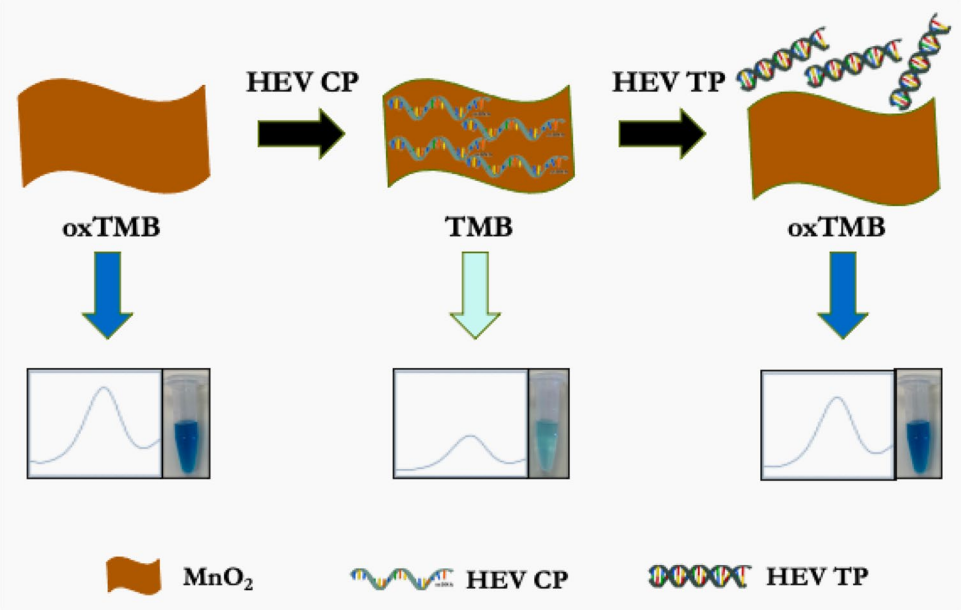

Scheme 1 Schematic diagram of MnO_2-TMB system for the colorimetric sensing of HEV

Synthesis of MnO_2 nanosheets

Potassium permanganate ($KMnO_4$) was used for the synthesis of MnO_2 nanosheets through a thermal decomposition method with slight modification from literature [30]. Briefly, 2 g of $KMnO_4$ was transferred into a porcelain crucible and was heated for 4 h at 500 °C in air and then cooled at room temperature. The product was harvested by centrifugation at 10,000 rpm for 8 min, and the soluble byproducts (K_3MnO_4 or K_2MnO_4) were removed by washing the product three times with distilled water. The MnO_2 was dried for 12 h in an electric oven at 60 °C. For further experiments, the final product was stored at room temperature.

Preparation of HEV-DNA@MnO_2

For the adsorption of DNA on the surface of MnO_2, 5 µL of 1 mg/mL MnO_2 (final concentration 20 µg/mL) was added to different concentrations (0, 0.5, 1.5, and 2.5 µM) of HEV capture probe. At room temperature, the mixture was vortexed for 2 h. The excess DNA was removed from the mixtures after incubation by centrifuging at 8000 rpm for 10 min. The pellet was kept at 0 °C for further use, while the supernatant was discarded.

Assay procedures

For detection of HEV, 2.5 µL of 1 mg/mL CP-modified MnO_2 (10 µg/mL final concentration) was added to 10 µL of different concentrations (0, 1 fM, 100 fM, 1 pM, 100 pM, 1 nM, and 100 nM) of HEV target probes. The mixtures were incubated for 30 min at 37 °C for binding of HEV capture probe and target probe. After 30 min of incubation, 235 µL of Na-Ac buffer (pH 3.5, 0.1 M) was added to the above mixtures. Finally, 2.5 µL of TMB (final concentration 1 mM) was added to a total of 250 µL reaction system to initiate the reaction. The absorption spectra were recorded from 350 to 800 nm using the excitation wavelength of 652 nm using a microplate reader. All the experiments were recorded in 3 replicates.

Characterizations

Powder X-ray diffraction (P-XRD) patterns were recorded using Bruker D8 Diffraction system with a Cu Kα source ($\lambda = 0.1541$ nm). The surface morphology of the prepared materials was investigated using TEM JEM-2100Plus transmission electron microscopy. Through N_2 adsorption desorption analysis utilizing a BET analyser, the surface area of the MnO_2 was measured. The DNA adsorption on MnO_2 was confirmed by atomic force microscopy (AFM) from Park NX10 SICM. A microplate reader (Cytation 5 Biotek) was used to examine the oxidase-like catalytic activities of the prepared material and TMB substrate. Zeta potentials of MnO_2 nanosheets, DNA, MnO_2-CP, and MnO_2-CP-TP were recorded using Zetasizer [Malvern Panalytical-UK, Nano ZS].

Results and discussion

Characterizations of MnO_2 nanosheets

MnO_2 nanosheets were synthesized through a facile one step thermal decomposition route. As displayed in Fig. 1,

the transmission electron microscopy images of MnO_2 nanosheets exhibited a typical two-dimensional layer structure and displayed multiple folds and wrinkled like sheet structure. The high surface-to-volume ratios of ultra-thin sheets could provide large specific surface area and allowing easy contact between reactant molecules and the active sites of nanosheets, thus providing enhanced catalytic activities as well as unique optical properties. High-resolution TEM images (Fig. 1C), shows that obtained nanosheets are free of any particle on surface. The TEM of MnO_2 nanosheets at 1 µm scale showing overall view is demonstrated in ESI (Fig. S1) and the size distribution at 200 nm scale in ESI (Fig. S2). From the HRTEM image, the d-spacing was analyzed and found to be around ~ 0.38 nm, which corresponds to the (002) plane displayed in Fig. 1D.

The energy-dispersive X-ray (EDS) spectra obtained using TEM microscope shows that Mn and O elements are present in MnO_2 nanosheets. The atomic percentage of Mn and O was approximately 25.40% and 74.60%, respectively, as shown in ESI, Fig. S3 and Fig. S4. This confirms successful formation of MnO_2 nanosheets.

The crystal structures and phase information of MnO_2 nanosheets are acquired from powder X-ray diffraction (PXRD) pattern in Fig. 2A. The diffraction peaks are considerably broadened due to noncrystalline nature of as-synthesized materials. The diffraction pattern observed at 2Θ of 11.8°, 24.9°, 36.4°, 41.4°, and 66.6° are corresponding to (211), (301), (600), and (002) crystal planes, respectively, which corresponds to tetragonal MnO_2 (JCPDS 44–0141). The minor variations in the distances between nanosheets in various restacked 2D structures can be used to explain the small variations in the (002) diffraction peak angles. By measuring the surface area by N_2 adsorption–desorption analysis using a BET analyzer, the results of the surface characteristics studies are shown in Fig. 2B, C, and D. The curves shows the type IV isotherm profiles [31]. Such profiles reveal two types of characteristics of the surface: (1) mesoporous structure and (2) unrestricted multilayer adsorption of the materials. It was found that the surface area of the material was 12.939 $m^2\ g^{-1}$. But it was interesting to know that the pore volume was more prominent with an average pore diameter of 19.895 nm. Such a large pore diameter is more suitable for catalytic processes, while the surface area of MnO_2 with capture probe and target probe were 19.71 $m^2\ g^{-1}$ and 14.76 $m^2\ g^{-1}$, respectively, which also confirms the adsorption and desorption of capture and target probes.

To further understand the morphology and adsorption of HEV-DNA on the surface of MnO_2 nanosheets, the atomic force microscopy (AFM) was used. From the AFM micrographs (Fig. 3A–C), the MnO_2 produced from thermal decomposition method shows the root mean square (RMS) surface roughness around 0.0043 µm (Fig. 3A), whereas

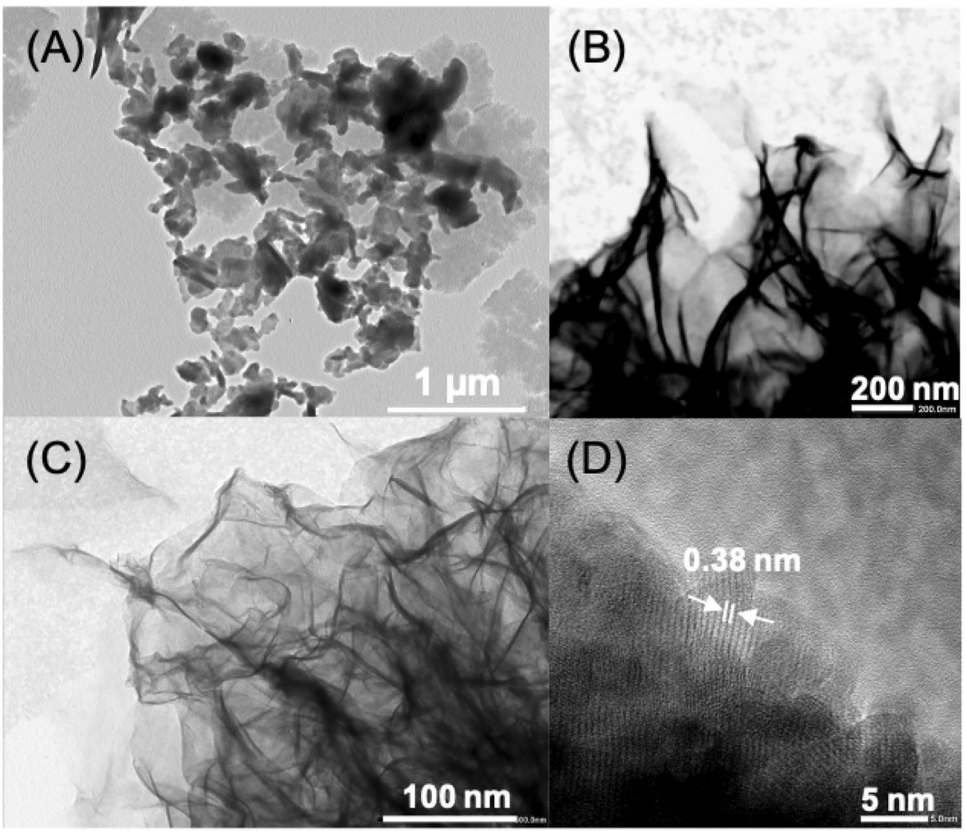

Fig. 1 TEM image of the MnO_2 nanosheets at different scales (**A**) 1 µm, (**B**) 200 nm, (**C**) 100 nm. (**D**) shows the d-spacing from the HRTEM image of MnO_2 nanosheets

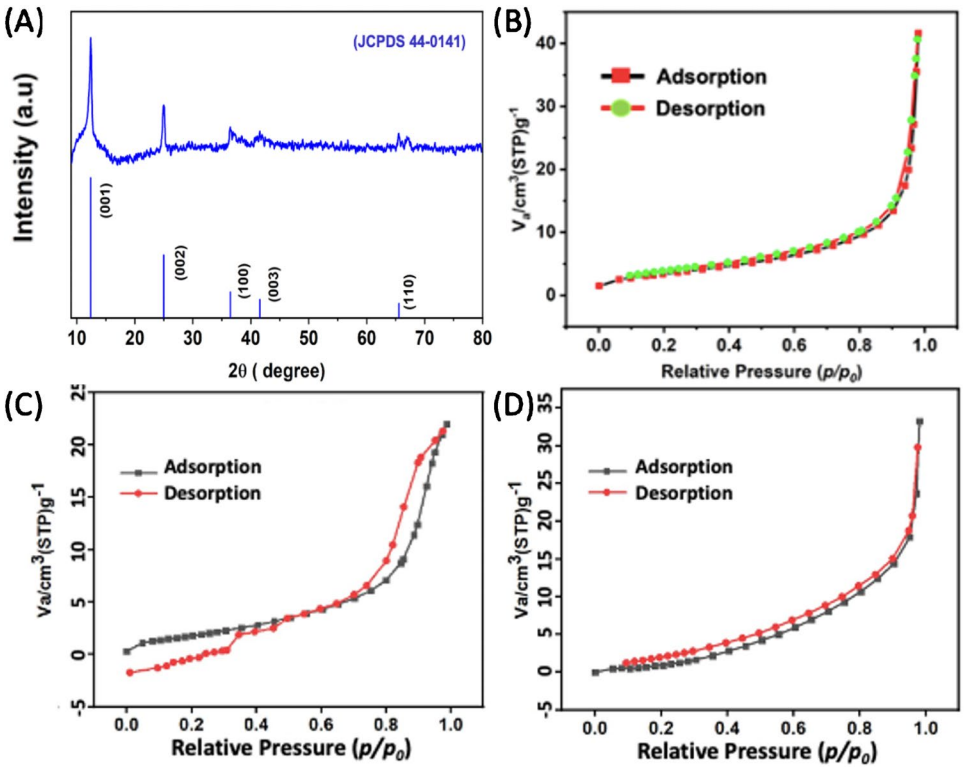

Fig. 2 **A** X-ray diffraction patterns of the synthesized MnO_2 nanosheets. **B** Nitrogen adsorption and desorption isotherms of the MnO_2 nanosheets, **C** MnO_2 with capture probe, and **D** MnO_2 with capture and target probes

ssDNA modified MnO_2 nanosheets attained a surface roughness 0.1916 µm (Fig. 3B). The change in morphology and surface roughness of MnO_2 nanosheets and ssDNA modified MnO_2 nanosheets clearly indicates that ssDNA adsorbed on the surface of MnO_2 nanosheets. The wavey kind structure was produced on the surface of MnO_2 representing the adherence of ssDNA and almost covered the area of the scan (Fig. 3B). Upon the addition of target DNA, it's interacted with ssDNA on the surface of MnO_2 nanosheets. The resulting hybridized DNA released from the surface of MnO_2 nanosheets. However, some unhybridized DNA is still adhered on the surface of MnO_2 nanosheets which can be seen as wavy kind of appearance on surface of the MnO_2 nanosheet as shown in Fig. 3C. The RMS roughness of HEV CP-modified MnO_2 + HEV TP is 0.0155 µm which confirm the adsorption and desorption of DNA on MnO_2 nanosheets.

This was further confirmed by zeta potential analysis of all the three materials along with the ssDNA. Unmodified MnO_2 nanosheets shows a zeta potential of − 39.6 mV, and ssDNA was − 17.4 mV. After modification with ssDNA, it was found that the zeta potential was increased to − 55.3 mV. Upon adding the target DNA to the system, the hybridized DNA was released from the surface, and the zeta potential was decreased again to − 44.8 mV which is almost closer

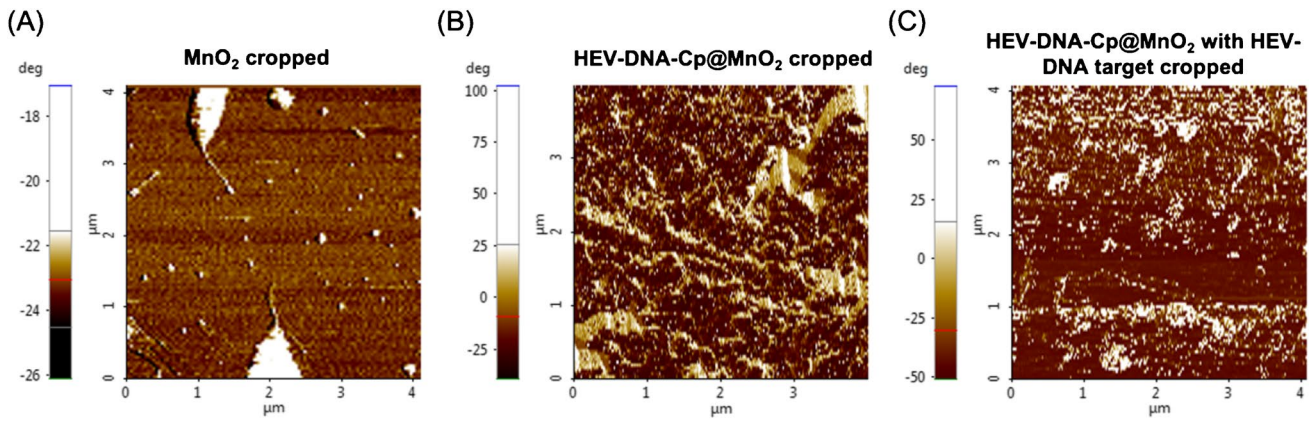

Fig. 3 **A** AFM images of the MnO_2 nanosheets, **B** MnO_2 + HEV CP, and **C** HEV CP-modified MnO_2 + HEV TP

to the value of unmodified MnO_2 zeta potential. This demonstrates that the majority of the ssDNA has been released while a small portion of unhybridized DNA is still remaining on the surface of MnO_2 nanosheets Fig. 4A. Furthermore, the HEV capture probe was labeled with Cy3 dye. A 2.5 µM of Cy3-labeled HEV CP was mixed with 10 µg/mL MnO_2 catalyst in Na-Ac buffer (pH 3.5, 0.1 M). The fluorescence was recorded in the absence and presence of HEV target probe as shown in Fig. 4B. The bare MnO_2 did not show fluorescence, while a high fluorescence was observed for MnO_2-CP demonstrating that MnO_2 is successfully modified with HEV DNA. But when HEV target was added into the system, the target probe hybridized with capture probe and released from the surface; hence, a decrease in the fluorescence was observed.

Proof of concept and verifications

In the presence of DNA, the surface of MnO_2 nanosheets can be masked that inhibits the biomimetic oxidase-like activity of MnO_2 nanosheets. DNA affects the catalytic activity of the MnO_2 nanosheets; it adsorbs on the surface of MnO_2 nanosheets via the negatively charged phosphate backbone [32] and by van der Waals force of interaction between the surface of MnO_2 material and nucleobases of DNA [33] and, thus, reasonably inhibits the oxidase-like activity of MnO_2 [34]. Encountering the HEV target DNA, the complementary target ssDNA is hybridized with the capture ssDNA probe, between the densely negatively charged phosphate backbones, the nucleobases are buried, and double-strand DNA (dsDNA) conformation is produced. By employing conserved sequences, no cross-reactivity existed because of specific complementarity. The dsDNA conformation can reduce the intensity of the Van der Waals interaction between dsDNA and the MnO_2 surface and inhibit interactions between nucleobases and material surfaces [35]. As a result of the electrostatic repulsion between dsDNA and MnO_2, the system's oxidase activity will recover as dsDNA is released from the surface of MnO_2 (Scheme 1). The basic principle behind the colorimetric sensing of HEV is based on the biomimetic oxidase-like activity of MnO_2 nanosheets. As shown in Fig. 5A, the TMB was colorless with no characteristic absorbance from 350 to 800 nm. After adding the as-prepared MnO_2 nanosheets, the oxidation of the colorless TMB produced a blue-colored product (oxTMB) as can be seen in the inset of Fig. 5A and giving a high absorbance peak. However, after the addition of the HEV capture probe into the MnO_2-TMB system, the absorbance at 652 nm was decreased by hindering the oxidation of TMB to oxTMB shown in Fig. 5B. This can be attributed to the adsorption of the HEV capture probe on the basal plane of MnO_2 through the negatively charged phosphate backbone [34]. The oxidation of TMB to oxTMB would be reduced as a result of covering the surface area of MnO_2 nanosheets, leading to the inhibition of biomimetic activity. Consequently, the intensity of the 652 nm absorbance reduced. However, there is some incomplete surface coverage of captured ssDNA on MnO_2 nanosheets for catalytic reaction which gives absorbance peak at 652 nm. But, upon the addition of target DNA to the MnO_2-TMB-HEV-CP system, the target probe binds to the capture probe on the surface of MnO_2 because of DNA hybridization. Hence, the hybridized DNA from the surface of MnO_2 is released, and the oxidase-like activity of the MnO_2 is recovered. Confirmation of the feasibility of the target sensing approach through visual observations can be seen in ESI, Fig. S5. Without the use of H_2O_2, this efficient reaction between the TMB substrate and MnO_2 nanosheets offers tremendous stability and reproducibility. These results established the practicality of this colorimetric sensing mechanism and applied it to the detection of HEV target probe.

Optimization of assay conditions

For the highly throughput results of the HEV detection sensor, the critical parameters such as pH, MnO_2, and HEV capture probe were studied systematically to establish the optimal conditions. The concentration of MnO_2 was investigated to determine the optimum concentration for high oxidase-like activity. Different MnO_2 concentrations (0, 10, 20, 40,

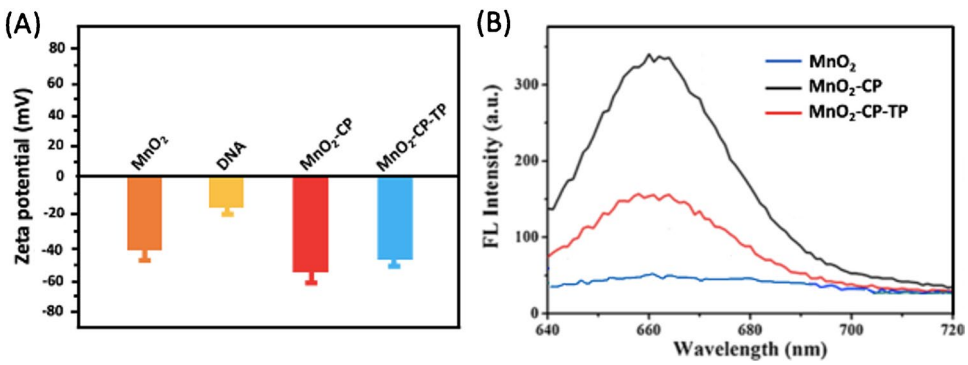

Fig. 4 Zeta-potential analysis of **A** MnO_2 nanosheets, ssDNA, MnO_2-CP and in the presence (MnO_2-CP-TP) of the HEV target probe. **B** Fluorescence spectra of MnO_2 nanosheets, MnO_2-CP and presence of the HEV target probe (MnO_2-CP-TP)

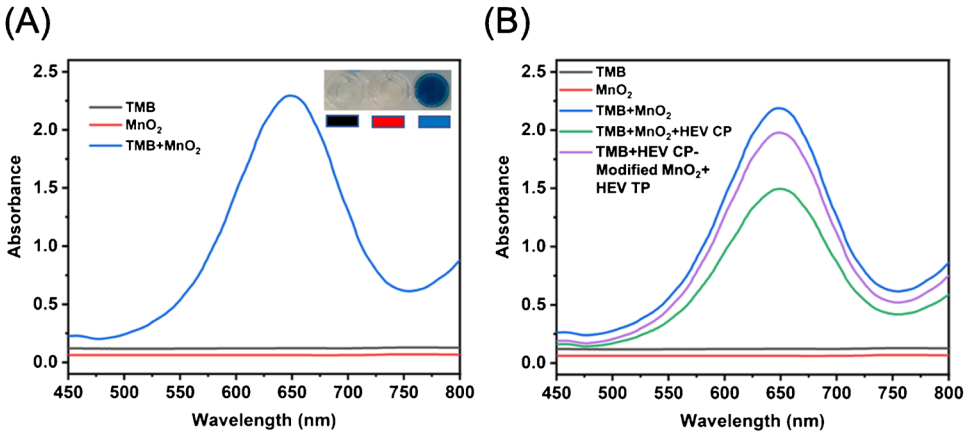

Fig. 5 UV–visible absorption spectra of (**A**) only TMB, only MnO_2 and TMB + MnO_2. Inset of **A** is the visual observations. (**B**) The mixtures (TMB, MnO_2, TMB + MnO_2, TMB + MnO_2 + HEV CP and TMB + HEV CP-modified MnO_2 + HEV TP) in the presence of TMB (1 mM) and MnO_2 (20 µg/mL)

and 60 µg/mL) were added to MnO_2-TMB reaction system. In ESI, Fig. S6A depicts that the UV–visible absorbance peak intensity centered at 652 nm increases with increasing concentrations of MnO_2. There was a linear relationship between MnO_2 concentration and absorption spectra at 652 nm with the regression coefficient ($R^2 = 0.999$) as shown in ESI, Fig. S6B. For high accuracy, we employed 10 µg of MnO_2 for further experiments of HEV detection.

As the pH value is critical for the high oxidase-like activity of MnO_2, Na-Ac buffer of pH range from 3 to 6 was studied. As presented in ESI, Fig. S7, the absorbance spectra of the reaction system decreased steadily with increasing pH value. MnO_2 exhibits high enzymatic activity in mildly acidic conditions, and MnO_2 nanosheets have a high oxidation capability [36]. So, Na-Ac buffer of pH 3.5 was selected for further experiments.

Adsorption of HEV-DNA on MnO_2 nanosheets

To investigate the application of MnO_2-TMB sensing platform for the detection of HEV, the system was first applied to investigate the adsorption of HEV capture probe on MnO_2 surface. Under the optimum experimental conditions, different concentrations of HEV capture probe in the range of 0–2.5 µM were applied to adsorb on the surface of MnO_2. The concentrations of HEV capture probe have a huge effect on the catalytic activity of MnO_2. As the concentration of HEV capture probe increased from 0 to 2.5 µM, the absorbance spectra at 652 nm decreased as illustrated in Fig. 6A. The color of the reaction was considerably changed from dark blue to light blue which was also confirmed by visual observations shown in Fig. 6B. The HEV capture probe was physically adsorbed successfully by MnO_2 via phosphate backbone of DNA which is often bound by some nanoparticles [37]. In literature, it is reported that due to large number of terminal phosphate groups, its binding affinity to nanoparticles is higher [38]. DNA affects the catalytic activity of the nanomaterial; it adsorbs on the surface of the nanomaterial via the negatively charged phosphate backbone [32]. This indicates that the adsorption of HEV capture probe masked the surface of MnO_2, so less MnO_2 surface is available for the catalytic oxidation of TMB and hence decreases the absorbance spectra at 652 nm. When the concentration of HEV capture probe increased, the absorbance spectra at 652 nm decreased. Figure 6C shows that there is an indirect relationship between the change in absorbance and the HEV capture probe concentration from 0 to 2.5 µM with a correlation coefficient of 0.984. Figure 6D shows a clear difference in the absorbance spectra of TMB + MnO_2 and TMB + MnO_2 + HEV CP.

Analytical performance of the sensor for HEV detection

The proposed colorimetric sensor was also employed to detect HEV under the ideal experimental conditions. With increasing the concentration of HEV target probe ranging from 1 fM to 100 nM, the absorbance spectra at 652 nm of the sensing platform was gradually increased as displayed in Fig. 7A. As the concentration of HEV target probe increases, more number of target probes bind with capture probe, and the surface of MnO_2 is unmasked. Hence, the oxidase-like activity of the MnO_2 is recovered by the oxidation of TMB to oxTMB. The absorbance spectra at 652 nm are intensified. Figure 7B shows the visual confirmation of the increased oxidation of TMB by MnO_2. With the increasing concentration of target probes in the sensing system, more capture probes are released from the surface of MnO_2. This confirms more availability of MnO_2 for the oxidation of TMB and the color of the sensing system changes from light blue to dark blue. Figure 7C illustrates a linear relation of change in absorbance spectra and the target probe concentration from 1 fM to 100 nM with the regression coefficient of 0.998. The absorbance spectra at 652 nm were directly related to the sensing of HEV; this correlates linearly with the concentration of HEV target probe. The LOD was calculated to

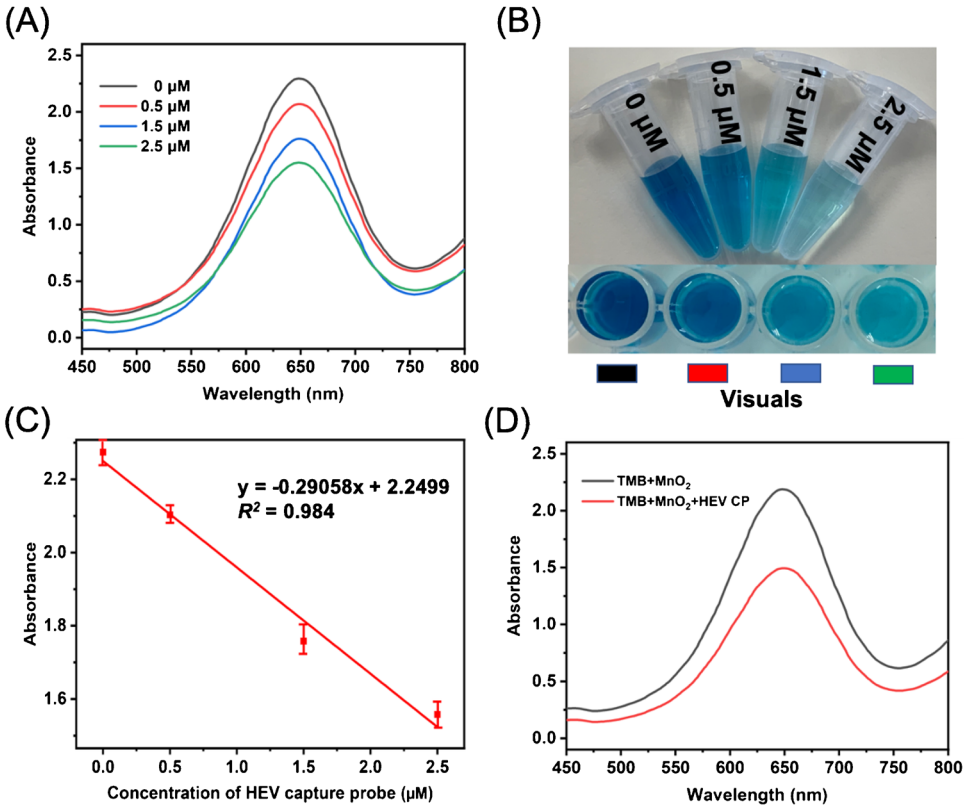

Fig. 6 UV–visible absorption spectra of **A** varied concentrations (0, 0.5, 1.5, and 2.5 µM) of DNA adsorption on MnO_2 in presence of TMB (1 mM) and MnO_2 (20 µg/mL). **B** shows the visual representations of adsorption of different concentrations of DNA on MnO_2 resulting in decrease oxidation of TMB. **C** The liner calibration between the different concentrations of DNA adsorption on MnO_2 and the decrease in TMB oxidation. **D** UV–visible absorption spectra of TMB + MnO_2 sensing system in the absence (black) and presence (red) of adsorbed DNA on MnO_2

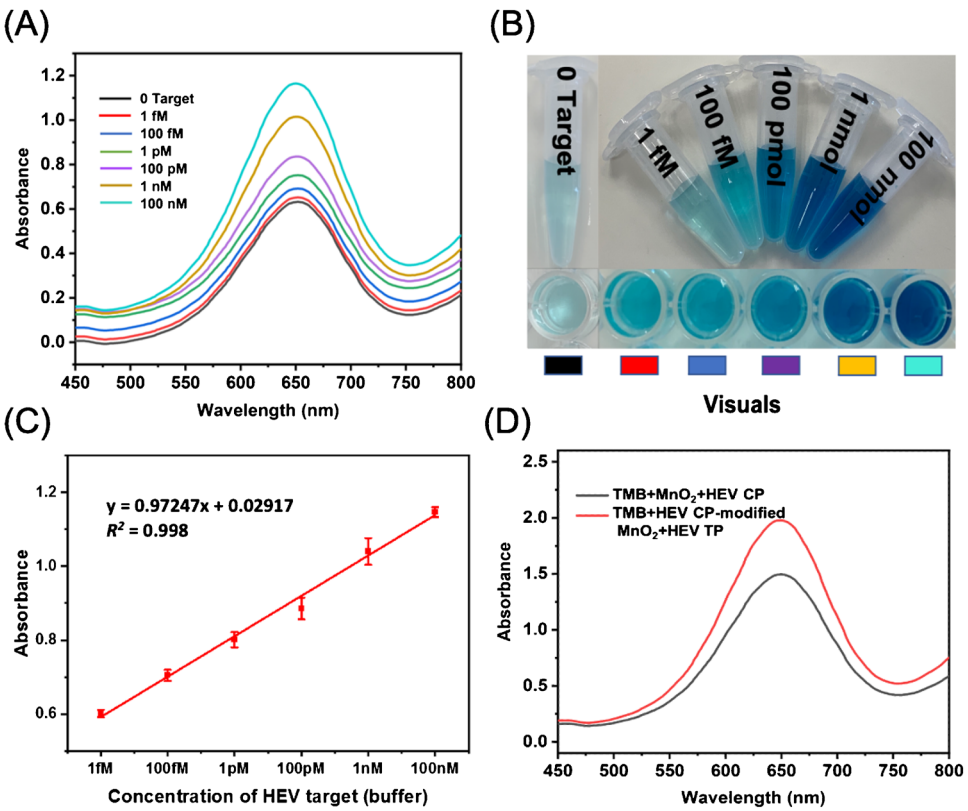

Fig. 7 A UV–visible absorption spectra for detection of different concentrations (0, 1 fM, 100 fM, 1 pM, 100 pM 1 nM, and 100 nM) of HEV target in presence of TMB (1 mM) and MnO_2 (10 µg/mL). **B** Visual illustrations of detection of different concentrations of HEV target probes leading to recovery of oxidase-like catalytic activity of MnO_2. **C** Displays the linear calibration of detection of HEV target probes and recovery of oxidase-like activity of MnO_2. **D** UV–visible absorption spectra of TMB-MnO_2 sensing system in the absence (red) and presence (black) of HEV target probe and 20 µg/mL of MnO_2 catalyst

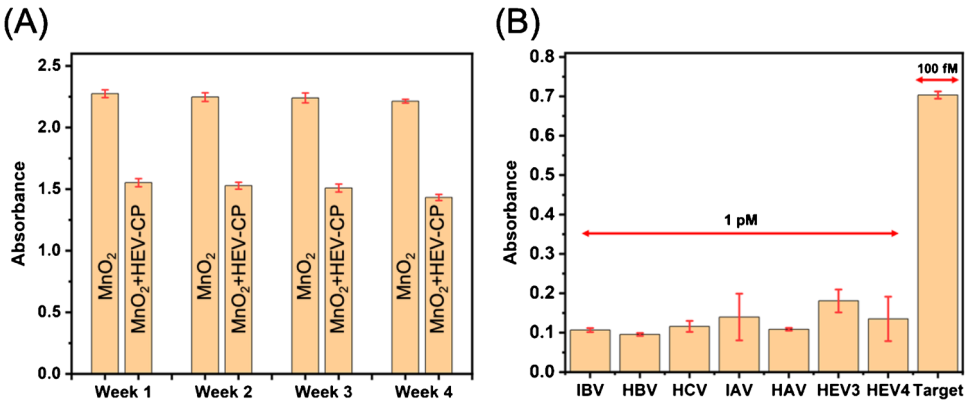

Fig. 8 Stability and selectivity of the developed sensor. **A** Stability of oxidase activity of MnO_2 nanosheets and hindering oxidase activity of MnO_2 nanosheets by HEV-CP in the presence of TMB (1 mM), MnO_2 (20 µg/mL), and HEV-CP (2.5 µM). **B** Selectivity of HEV target (100 fM) over potential interferences. IBV, HBV, HCV, IAV, HAV, HEV-3, HEV-4 (1 pM). The incubation time selected was 5 min. Error bar represents the standard deviation for three determinations

be 3.26 fM based on the standard deviation of the response (Sy) of the curve and the slope of the calibration curve (S) at levels approximating the LOD according to the formula: LOD = 3.3(Sy/S). The LOQ was calculated to be 36.08 fM on the basis of standard deviation of the response (SD) and the slope of the calibration curve (S) according to the formula: LOQ = 10(Sy/S). The standard deviation of the response was determined based on the standard deviation of y-intercepts of the regression lines. The results are comparatively better than those of earlier reports tabulated in Table S1 in ESI. There is an obvious change in the absorbance spectra of TMB + MnO_2 + HEV CP and TMB + HEV CP-modified MnO_2 + HEV TP. In TMB + MnO_2 + HEV CP sensing system, most of the MnO_2 surface is hindered by the adsorbed capture probe, so fewer MnO_2 active sites are available to catalyze the TMB present in the reaction system. This can also be attributed to the presence of bigger pore size and volume. These can also provide necessitated active sites possible to even load the ssDNA to MnO_2, and this is evident from BET analysis. As the target probe is added into the system, the capture probe binds with the target probe because of their complementarity with each other. Hence, the oxidase activity of MnO_2 is recovered for the oxidation of TMB as shown in Fig. 7D.

Stability and selectivity of the biosensor

In order to assess the reliability of the developed sensor, the cyclic stability tests of MnO_2 and MnO_2 + HEV-CP were performed at a 1-week interval for a period of 1 month as displayed in Fig. 8A. It indicates that our prepared material exhibits good catalytic activity and stability over a month without affecting its primary performance. The selectivity of this sensing system was subsequently studied by monitoring the change in absorbance activity with other interfering molecules. To assess the specificity of the suggested sensor, we selected other mismatched DNA sequences such as IBV, HBV, HCV, IAV, HAV, HEV-3, and HEV-4 as shown in Table S2. The concentrations of these interferents were set as 1 pM, while 100 fM concentration was set for HEV target (equivalent to 0.1 pM). As shown in Fig. 8B, due of the non-specific interaction with the HEV capture probe, the biosensor responses to

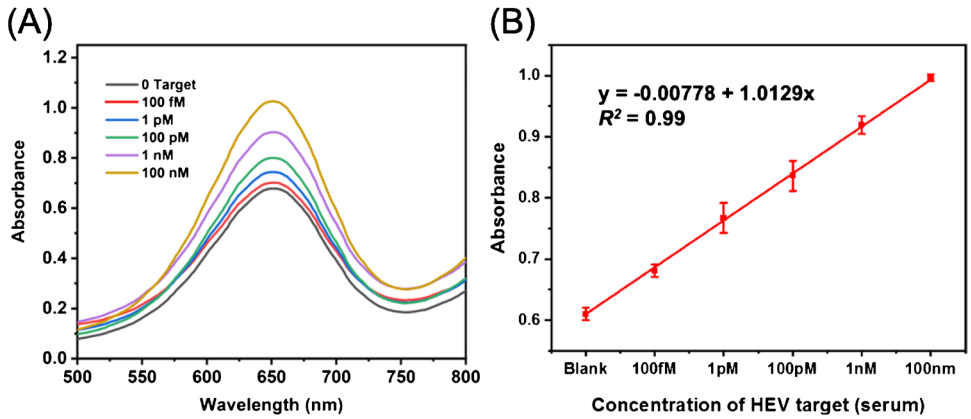

Fig. 9 Sensor performances for different concentrations of HEV analytes in serum. **A** UV–visible absorption spectra of detection of different concentrations (100 fM, 1 pM, 100 pM, 1 nM, and 100 nM) of HEV target in serum in presence of TMB (1 mM) and MnO_2 (10 µg/mL). **B** depicts the linear calibration of detection of HEV target in human serum samples

Table 1 Detection of HEV target in serum sample with this sensor

Sample	Added	Detected	Recovery (%)	RSD (%, $n=3$)
HEV	100 fM	99 fM	99.0	4.93
HEV	1 pM	0.98 pM	98.0	3.57
HEV	100 pM	97.5 pM	97.5	5.01
HEV	1 nM	0.99 nM	99.0	6.36
HEV	100 nM	101.5 nM	101.5	4.30

the other virus sequences are much lower, even though they were in higher concentration than HEV. This makes our developed sensor unique to the target analyte. This confirms that our developed colorimetric sensor possesses excellent specificity and selectivity for HEV detection.

Analytical performance in spiked serum samples

To further explore the analytical performance of our colorimetric sensor in complex biological samples, the human serum obtained from Sigma-Aldrich was diluted tenfold after centrifugation. Then, the diluted serum sample was combined with 10 µL of various HEV DNA concentrations (100 fM, 1 pM, 100 pM, 1 nM, and 100 nM) and incubated for 30 min at 37 °C. To examine whether the developed sensor could be applied for the sensing of HEV in a real sample, the absorbance responses are tested in spiked serum samples. As depicted in Fig. 9A, the biosensor responses display a similar tendency of increasing absorbance with increasing concentrations (100 fM–100 nM) of HEV targets as in the buffer. The LOD and LOQ were calculated to be 9.32 fM and 28.24 fM, respectively. Figure 9B shows a linear relation of change in absorbance spectra vs different concentrations of target HEV (100 fM, 1 pM, 100 pM, 1 nM, and 100 nM) with the regression coefficient value of 0.99 ($n=3$). The absorbance spectra of target detection in Na-Ac buffer and human serum are shown in ESI, Fig. S8. The recoveries of HEV target DNA ranged from 97.5 to 101.5% tabulated in Table 1, proving that the suggested method may be used to diagnose HEV in patients without the need for complex pretreatments.

Conclusion

In conclusion, a label-free, highly sensitive colorimetric sensing system was developed to identify the Hepatitis E virus. The strategy has relied on effective biomimicking oxidase activity of MnO_2 nanosheets. This approach can catalyze the oxidation of TMB into oxTMB that can be visualize by the naked eye as a clear absorption peak at 652 nm with a colorimetric change from colorless to blue product. The addition of HEV DNA capture probe to the system leads to the inhibition of biomimetic oxidase activity due to adsorption of the DNA on the surface of MnO_2 nanosheets. The oxidase activity was regained by the introduction of HEV target probe. HEV target probe binds to the HEV capture probe, thus hindering the interaction between the MnO_2 surface and DNA. This releases the DNA from the surface exposing them to more catalytic surface sites, recovering the oxidase-like activity. The assay was also used to quantify HEV target DNA in spiked serum samples with high accuracy showing its feasibility and reliability. Therefore, this simple approach could offer an easy, robust, and label-free sensing platform for biological and clinical diagnostic applications.

Supplementary Information The online version contains supplementary material available at https://doi.org/10.1007/s00216-022-04461-1.

Acknowledgements Naveed Alam gratefully acknowledges Petchra Pra Jom Klao PhD Research scholarship, King Mongkut's University of Technology Thonburi (KMUTT). All the authors acknowledge the efforts of Dr. Asma Gul during the proofreading of the revised manuscript.

Declarations

Conflict of interest The authors declare no competing interests.

References

1. Emerson SU, Purcell RH. Hepatitis E virus. 2003;13(3):145–54.
2. Kaba M, Moal V, Gérolami R, Colson P. Epidemiology of Mammalian Hepatitis E Virus Infection. Intervirology. 2013;56(2):67–83.
3. Rein DB, Stevens GA, Theaker J, Wittenborn JS, Wiersma ST. The global burden of hepatitis E virus genotypes 1 and 2 in 2005. Hepatology. 2012;55(4):988–97.
4. World Health Organisation Hepatitis E. (2018) Available at: https://www.who.int/news-room/fact-sheets/detail/hepatitis-e. Accessed 1 February 2019
5. Martin-Latil S, Hennechart-Collette C, Guillier L, Perelle S. Method for HEV detection in raw pig liver products and its implementation for naturally contaminated food. Int J Food Microbiol. 2014;176:1–8.
6. Khoris IM, Takemura K, Lee J, Hara T, Abe F, Suzuki T, et al. Enhanced colorimetric detection of norovirus using in-situ growth of Ag shell on Au NPs. Biosens Bioelectron. 2019;126:425–32.
7. Chen W, Li S, Wang J, Sun K, Si Y. Metal and metal-oxide nanozymes: bioenzymatic characteristics, catalytic mechanism, and eco-environmental applications. Nanoscale. 2019;11(34):15783–93.
8. Singh S, Dosani T, Karakoti AS, Kumar A, Seal S, Self WT. A phosphate-dependent shift in redox state of cerium oxide nanoparticles and its effects on catalytic properties. Biomaterials. 2011;32(28):6745–53.
9. Liu B, Liu J. Surface modification of nanozymes. Nano Res. 2017;10(4):1125–48.
10. Lin Y, Ren J, Qu X. Catalytically active nanomaterials: a promising candidate for artificial enzymes. Acc Chem Res. 2014;47(4):1097–105.

11. Hassan SSM, Sayour HEM, Kamel AH. A simple-potentiometric method for determination of acid and alkaline phosphatase enzymes in biological fluids and dairy products using a nitrophenylphosphate plastic membrane sensor. Anal Chim Acta. 2009;640(1):75–81.
12. Shi J, Guo J, Bai G, Chan C, Liu X, Ye W, et al. A graphene oxide based fluorescence resonance energy transfer (FRET) biosensor for ultrasensitive detection of botulinum neurotoxin A (BoNT/A) enzymatic activity. Biosens Bioelectron. 2015;65:238–44.
13. Xi Q, Zhou D-M, Kan Y-Y, Ge J, Wu Z-K, Yu R-Q, et al. Highly sensitive and selective strategy for microRNA detection based on WS2 nanosheet mediated fluorescence quenching and duplex-specific nuclease signal amplification. Anal Chem. 2014;86(3):1361–5.
14. Liu J, Tang D, Chen Z, Yan X, Zhong Z, Kang L, et al. Chemical redox modulated fluorescence of nitrogen-doped graphene quantum dots for probing the activity of alkaline phosphatase. Biosens Bioelectron. 2017;94:271–7.
15. Gopi PK, Ngo DB, Chen S-M, Ravikumar CH, Surareungchai W. High-performance electrochemical sensing of hazardous pesticide Paraoxon using BiVO4 nano dendrites equipped catalytic strips. Chemosphere. 2022;288: 132511.
16. Zhang X-L, Zheng C, Guo S-S, Li J, Yang H-H, Chen G. Turn-on fluorescence sensor for intracellular imaging of glutathione using g-C3N4 nanosheet–MnO2 sandwich nanocomposite. Anal Chem. 2014;86(7):3426–34.
17. Lin T, Zhong L, Guo L, Fu F, Chen G. Seeing diabetes: visual detection of glucose based on the intrinsic peroxidase-like activity of MoS2 nanosheets. Nanoscale. 2014;6(20):11856–62.
18. Zhu C, Zeng Z, Li H, Li F, Fan C, Zhang H. Single-Layer MoS2-based nanoprobes for homogeneous detection of biomolecules. J Am Chem Soc. 2013;135(16):5998–6001.
19. Dong Y-l, Zhang H-g, Rahman ZU, Su L, Chen X-j, Hu J, et al. Graphene oxide–Fe3O4 magnetic nanocomposites with peroxidase-like activity for colorimetric detection of glucose. Nanoscale. 2012;4(13):3969–76.
20. Yuan Y, Wu S, Shu F, Liu Z. An MnO2 nanosheet as a label-free nanoplatform for homogeneous biosensing. Chem Commun. 2014;50(9):1095–7.
21. Xie J, Cao H, Jiang H, Chen Y, Shi W, Zheng H, et al. Co3O4-reduced graphene oxide nanocomposite as an effective peroxidase mimetic and its application in visual biosensing of glucose. Anal Chim Acta. 2013;796:92–100.
22. Tan Q, Zhang R, Kong R, Kong W, Zhao W, Qu F. Detection of glutathione based on MnO2 nanosheet-gated mesoporous silica nanoparticles and target induced release of glucose measured with a portable glucose meter. Microchim Acta. 2017;185(1):44.
23. Huang W, Deng Y, He Y. Visual colorimetric sensor array for discrimination of antioxidants in serum using MnO2 nanosheets triggered multicolor chromogenic system. Biosens Bioelectron. 2017;91:89–94.
24. HunsurRavikumar C, Nair GV, M. P R, Surareungchai W, Thakur A, Balakrishna RG. Biomass derived carbon dot decorated ssDNA for a 'turn-on' fluorescent assay for detection of Staphylococcus aureus MNase. New J Chem. 2021;45(13):5890–6.
25. Ma Z, Wu T, Li P, Liu M, Huang S, Li H, et al. A dual (colorimetric and fluorometric) detection scheme for glutathione and silver (I) based on the oxidase mimicking activity of MnO2 nanosheets. Microchim Acta. 2019;186(8):498.
26. Chen J, Wang Y, Wei X, Ni R, Meng J, Xu F, et al. A composite prepared from MnO2 nanosheets and a deep eutectic solvent as an oxidase mimic for the colorimetric determination of DNA. Microchim Acta. 2019;187(1):7.
27. Yang Q, Wang X, Peng H, Arabi M, Li J, Xiong H, et al. Ratiometric fluorescence and colorimetry dual-mode assay based on manganese dioxide nanosheets for visual detection of alkaline phosphatase activity. Sens Actuators, B Chem. 2020;302: 127176.
28. Liu J, Meng L, Fei Z, Dyson PJ, Zhang L. On the origin of the synergy between the Pt nanoparticles and MnO2 nanosheets in Wonton-like 3D nanozyme oxidase mimics. Biosens Bioelectron. 2018;121:159–65.
29. Ngo DB, Chaibun T, Yin LS, Lertanantawong B, Surareungchai W. Electrochemical DNA detection of hepatitis E virus genotype 3 using PbS quantum dot labelling. Anal Bioanal Chem. 2021;413(4):1027–37.
30. Komaba S, Kumagai N, Chiba S. Synthesis of layered MnO2 by calcination of KMnO4 for rechargeable lithium battery cathode. Electrochim Acta. 2000;46(1):31–7.
31. Ravikumar CH, M S, Mahto A, Nanjundaiah RT, Thippeswamy R, Teixeira SR, et al. Observation of oxo-bridged yttrium in TiO2 nanostructures and their enhanced photocatalytic hydrogen generation under UV/visible light irradiations. Mater Res Bull. 2018;104:212–9.
32. Kim HY, Ahn JK, Kim MI, Park KS, Park HG. Rapid and label-free, electrochemical DNA detection utilizing the oxidase-mimicking activity of cerium oxide nanoparticles. Electrochem Commun. 2019;99:5–10.
33. He D, He X, Wang K, Yang X, Yang X, Li X, et al. Nanometer-sized manganese oxide-quenched fluorescent oligonucleotides: an effective sensing platform for probing biomolecular interactions. Chem Commun. 2014;50(75):11049–52.
34 Pautler R, Kelly EY, Huang P-JJ, Cao J, Liu B, Liu J. Attaching DNA to nanoceria: regulating oxidase activity and fluorescence quenching. ACS Appl Mater Interface. 2013;5(15):6820–5.
35. Ge J, Ou E-C, Yu R-Q, Chu X. A novel aptameric nanobiosensor based on the self-assembled DNA–MoS2 nanosheet architecture for biomolecule detection. Journal of Materials Chemistry B. 2014;2(6):625–8.
36. He L, Wang F, Chen Y, Liu Y. Rapid and sensitive colorimetric detection of ascorbic acid in food based on the intrinsic oxidase-like activity of MnO2 nanosheets. Luminescence. 2018;33(1):145–52.
37. Liu B, Liu J. DNA adsorption by magnetic iron oxide nanoparticles and its application for arsenate detection. Chem Commun. 2014;50(62):8568–70.
38. Wang X, Lopez A, Liu J. Adsorption of phosphate and polyphosphate on nanoceria probed by DNA oligonucleotides. Langmuir. 2018;34(26):7899–905.